EasyChair Preprint

№ 7273

Aerodynamic Design and Numerical Analysis of Bi-Cambered Airfoil

Sashant Kapoor, Vipin Kumar, Harshit Shukla, Kumar Gaurav and Dalbir Singh

December 28, 2021

Aerodynamic Design and Numerical Analysis of Bi-cambered Airfoil

Sashant Kapoor[1, a)] Vipin Kumar[1, b)] Harshit Shukla[1,c)] Kumar Gaurav[1,d)] Dalbir Singh [2,e)]

[1] *Department of Aerospace Engineering, University of Petroleum and Energy Studies, Dehradun, India*
[2]*School of Aeronautical Sciences, Hindustan Institute of Technology and Science, Chennai, India*

[a)] kapoorsashant@gmail.com
[b)] sara.vipinkumar@gmail.com
[c)] hshukla21@gmail.com
[d)] kmar12791@gmail.com
[e)]dsinghcad@gmail.com

Abstract. With the advancement of aerodynamics shapes, designing an airfoil contour is still a basic structure in fluid machinery. The present research provides a design criterion for a stable airfoil at a high angle of attack. An improved airfoil contour has been designed with two ridges on the upper surface and a flat bottom-placed laterally to fluid flow, which is running from leading edge to trailing edge and is named a bi-cambered airfoil. The current aim of this research is to enhance the aerodynamic efficiency to meet the outcome of the useful results. Rather than a single reflexed cambered surface with one, two, or more convex or concave curves may be used in the design of an airfoil. Bi-camber surface airfoil tends to attach a boundary layer at the second cambered surface of the airfoil, which results in improving aerodynamic characteristics. These characteristics provide extensive possibilities in designing the airfoil for a high altitude aircraft where the stalling angle is low due to thin air and in wind turbines where the high angle of attack flow is common. Therefore, bi-cambered airfoil effectively lowers local Reynolds number is respect to boundary layer development.

Keywords – Bi-camber airfoil, aerodynamics characteristics, aerodynamic efficiency, airfoil contour, flow control, high angle of attack

Introduction

Till present time basic airfoil designed with only a single maximum camber at 25% of chord for subsonic aircraft and 50% of chord for supersonic aircraft, so to retain the flow streamlined over the airfoil profile study of boundary layer interaction with the outer flow field must be a purpose of research. Boundary layer effects can be aggravated mainly at high speeds, as shock waves' presence can be seen after the local pocket of supersonic flow over the lifting surface on the airfoil.

For the last few decades, a major subject to research in aerodynamics is flow control techniques over an aircraft. As modern civilian aircraft's cruise velocity is limited for fuel efficiency because of the drag penalty which occurs due to shock waves, which is technically termed as wave drag. To mark an additional improvement in fuel consumption, the flow control method tends to achieve an increment in the lift to drag ratio, which can be achieved by a decrement in the drag related to the shock waves in cruising flight conditions. Since there are numerous flow control methods which had been researched and practiced achieving accurate results, such flow control methods are passive control of flow at the foot of the shock by applying porous surface, a bump on airfoil surface near the shock, and active control flow control method by using mass suction or blowing of hot air[1]. Most conventional flow control methods are suction/blowing of air and contour bumps on the airfoil's upper surface. Stanewsky et al. [3] said that the most effective way to reduce wave drag on an airfoil is a contour bump at the shock region. The contour bump is beneficial as it replaces the isentropic compression from the normal transonic shock or would break down it into numerous weaker shocks [1]. Moreover, to control flow over an airfoil, additional energy input does not need for contour bump but in the case of suction/blowing of hot air additional energy is needed to reduce the wave drag

[3]. In past, there are numerous studies had been performed about the suction/blowing of hot air for improvement in the existing airfoil performance at subsonic speeds [4]. Near the rigid surface, the boundary layer keeps growing along the surface as long as the pressure gradient remains zero. For an adverse pressure gradient, static pressure increases in the flow direction which is a drastic increase in the thickness of the boundary layer. The effect of viscous force and adverse pressure gradient reduces airflow boundary layer region momentum, and effectiveness of these will follow for some considerable length on the airfoil surface and will create a halt in boundary layer growth and this would be termed as flow separation. If the airfoil is being avoided from flow separation near the trailing edge, the boundary layer remains attached to the surface and hence pressure drop is being eliminated near the airfoil trailing edge, and thus drag force will be decreased [2]. The main objective is to control the boundary layer over an airfoil which would result in an increment of lift force and decrease the drag force, and hence it will enhance the aerodynamic performance of the airfoil by delaying the stall and increasing the lift-to-drag ratio.

In this current paper, we analyzed and performed a study that is associated with bi-camber airfoil raised protuberance and concave section that is avoided as it generally impacts to reduce the aerodynamic performance. During this study, two control mechanisms named contour bump and injection/blowing of hot air are examined to reduce the effect shock wave and hence decrement of total drag on the airfoil. It may also adversely affects other design parameters of an airfoil to get improved fluid mechanics performance by using such flow control methods [5]. To optimize the aerodynamic performance for bi-camber on different parameters, some crucial parameters were decided such as maximum camber, cord length, maximum thickness, and the crest position for two ridges on airfoil upper surface and ridges location, and angles on which two ridges were designed. The ridges can be found symmetrical or asymmetrical, as it depends on the location of the upper surface ridges on the airfoil. However, an efficient method that is based on the optimization technique of the pressure gradient, this method is used to optimize the parameters of contour bump and the steady suction/blowing of hot air. These optimizations were carried out by CFD fluent solver. Since various airfoils profiles have been designed to support aerodynamic performance by inducing flow transition at an early stage of separation which leads to energizing the flow near the boundary so that it gives benefit to delay the flow separation. For example, a reduction in drag can be attained when airfoil stall performance is yielded, which leads to results an increment in lift force, but at the cost profile drag increment. Stall performance of an airfoil can be enhanced, which dually affects the drag and lift performance, but general performance characteristics can be improved for some angles of attacks or some Reynolds number, but at the same time accepting reduced performance for other angles of attacks [6].

To reduce the drag disadvantage bi-camber airfoil is designed smoothly along with using flow control methods. This type of profile could be useful in normal aircraft applications such as the use of trim tabs to fly aircraft at high angle of attack or flaps or any other applications like rotorcrafts and wind turbines where airfoils operated at a wide range of flight conditions, the advantage of bi-cambered airfoil would become more noticeable.

Methodology

Since there are very little research data available on bi-camber airfoil design we re-mapped airfoil using paper and designed an optimized flat base bi-camber airfoil with two ridges on the upper surface. Frederick et al. [7] suggest an innovative design of a bi-camber airfoil that records a stable performance parameter of the airfoil such as efficiency and high angle of attack. This airfoil is providing a design condition for favorable and adverse pressure gradients in between two ridges and maximizing flow to be attached further to the trailing edge and minimizing flow separation. To illustrate the basic design of bi-camber airfoil author describes some basic design characteristics in figure 1. Figure 1 demonstrates the profile of a bi-camber airfoil section 1 with leading-edge at 12, trailing edge at 13, and chord line at 14. Upper surface demonstrates a section divided into some major fractions 1,2,5,6,7,8,3. Leading-edge front section I (slope 1,2) and trailing edge rear section III (slope 3). The front and rear slopes are separated by a central section II comprised of slope segments 5,6,7,8 and with a minimum thickness in central section 10. The central section slopes are divided into two convex and two concave sections; rear-facing convex and concave division 5 and 6, forward-facing concave and convex sections 7 and 8. The divisions' combination consists of forward-facing slope 5,6 and rear-facing slope 7,8 and the two ridges with front and rear end maximum thickness 9,11. Using this type of front and rear slopes on the upper surface defined it as a bi-cambered airfoil surface. The four separated slopes on the upper surface of this airfoil incorporate pressure gradient in respect to fluid flow at zero degrees of angle of attack. The convex and concave slope of the first ridge or section I results in a favorable pressure gradient and the front slope of a rear camber i.e., 5,6 results in us an adverse pressure gradient. For second elevation curve consists of a forward-facing slope, 7-8 which is responsible for favorable pressure gradient at the rear end, and a rear-facing slope or section III results in a final adverse pressure gradient. The lower surface is a flat surface that only has a single convex section for the entire length of the lower surface and resulting, in a favorable pressure gradient at the first half section of the airfoil, and resulting in an adverse pressure gradient, to the rest of the section. The lower surface contains only a single raised curve 4.

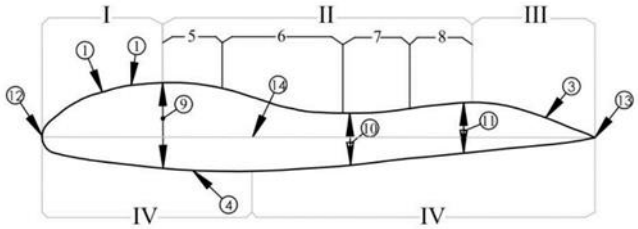

Figure 1 Descriptive view of Bi-camber airfoil

Using Q-blade software, the author designed the bi-camber airfoil in the preliminary phase. Q-blade is based on Blade Element Momentum (BEM) method. To design a specific definition for such airfoil, a scalar objective function doesn't have any need but some expertise must be required to identify the potential problems So, during the preliminary design of the bi-camber airfoil, the author adopts two methods i.e., direct method and inverse method. The direct design method implies direct airfoil designing which involves the geometric section specification, pressure calculation, and performance of airfoil. The inverse methods which author adapts to further design and analysis of an airfoil. As inverse design can be explained with the help of an example, a thin airfoil theory can be used to solve for the shape of the camber line that produces a specified pressure difference on an airfoil in potential flow and design problem starts when an author has somehow defined an objective for the airfoil design. So, using the inverse method author re-mapped the existing bi-camber and analyzed the airfoil which is then compared with commonly known airfoils.

Further, the author used ANSYS fluent software to analyze the flow over a bi-camber airfoil. According to the requirement and outcome author reviewed some research on various turbulence models.

RNG K-ε model: RNG k-epsilon model is developed using mathematical methods known as Re-Normalization Group which take account of turbulent motion at different existence scales. This method is generally used in the simulation of flows in rotating cavities.

Equation 1 - Turbulent kinetic energy k

$$\frac{\partial \rho k}{\partial t} + \frac{\partial \rho k u_i}{\partial x_i} = \frac{\partial}{\partial x_j}\left[\frac{\mu_t}{\sigma_k}\frac{\partial k}{\partial x_j}\right] + 2\mu_t \mathrm{EijEij} - \rho\varepsilon \quad (1)$$

Equation 2 – dissipation ε

$$\frac{\partial \rho \varepsilon}{\partial t} + \frac{\partial \rho \varepsilon u_i}{\partial x_i} = \frac{\partial}{\partial x_j}\left[\frac{\mu_t}{\sigma_k}\frac{\partial \varepsilon}{\partial x_j}\right] + C_1\varepsilon\frac{\varepsilon}{k}2\mu_t \mathrm{EijEij} - C_2\varepsilon\rho\frac{\varepsilon^2}{k} \quad (2)$$

K-ω turbulence model: It is similar to the k-epsilon model, but the k-omega model uses turbulent energy dissipation rate instead of dissipation equation. Using this model k determines energy turbulence and omega determines characteristic linear turbulence scale. This model is most sensitive to the boundary conditions in external flow and initial conditions of the turbulence level i.e., why it describes well near-wall flows, including with large eddy currents.

$$\frac{\partial \rho k}{\partial t} + \frac{\partial \rho u_j k}{\partial x_j} = \rho P - \beta^* \rho \omega k + \frac{\partial}{\partial x_j}\left[\left(\mu + \sigma_k \frac{\rho k}{\omega}\right)\frac{\partial k}{\partial x_j}\right] \quad (3)$$

$$\frac{\partial \rho \omega}{\partial t} + \frac{\partial \rho u_j \omega}{\partial x_j} = \frac{\alpha\omega}{k}P - \beta\rho\omega^2 + \frac{\partial}{\partial x_j}\left[\left(\mu + \sigma_k \frac{\rho k}{\omega}\right)\frac{\partial k}{\partial x_j}\right] + \frac{\rho\sigma_d}{\omega}\frac{\partial k}{\partial x_j}\frac{\partial \omega}{\partial x_j} \quad (4)$$

SST K-omega turbulence model: SST k-omega model is a shear stress transport turbulent model. This model consists of a combination of two models one is k-epsilon which works away from the wall and another is k-omega near the surface region of a test article. This model outputs good results in mixing layers at medium pressure gradient.

Equation 5 Kinematic Eddy Viscosity

$$\upsilon_T = \frac{a_1 k}{\max(a_1\omega, SF_2)} \quad (5)$$

Equation 6 Turbulence Kinetic Energy

$$\frac{\partial k}{\partial t} + U_j \frac{\partial k}{\partial x_j} = P_k - \beta^* k\omega + \frac{\partial}{\partial x_j}\left[(\upsilon + \sigma_k \upsilon_T)\frac{\partial k}{\partial x_j}\right] \quad (6)$$

Equation 7 Specific Dissipation Rate

$$\frac{\partial \omega}{\partial t} + U_j \frac{\partial \omega}{\partial x_j} = \alpha S^2 - \beta\omega^2 + \frac{\partial}{\partial x_j}\left[(\upsilon + \sigma_\omega \upsilon_T)\frac{\partial \omega}{\partial x_j}\right] + 2(1 - F_1)\sigma_{\omega^2}\frac{1}{\omega}\frac{\partial k}{\partial x_i}\frac{\partial \omega}{\partial x_i} \quad (7)$$

Analysis shows that turbulence model SST k-omega outputs the best results in the calculation of flows over an airfoil at a high angle to attack [8].

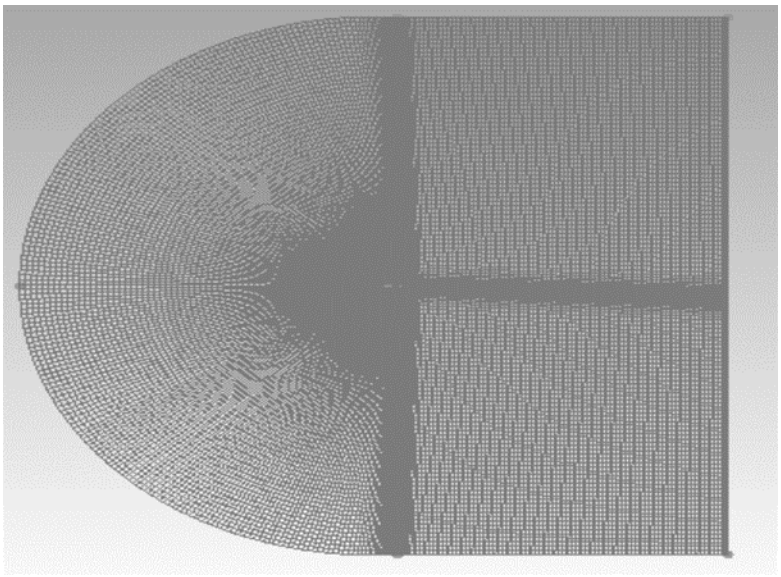

FIGURE 2 C-Type mesh over a Bi-camber airfoil

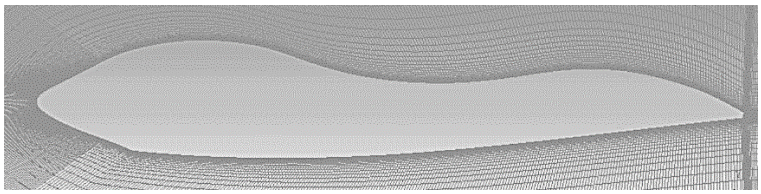

FIGURE 3 Meshing between two ridges of Bi-camber airfoil

Geometry and Grid Generation: The airfoil considered in this study is a Bi-camber airfoil with 18 cm of chord length. A C-type domain that follows the uniform pattern of structured mesh over a bi-cambered airfoil is created in ICEM CFD (version 15.0) with far-field boundaries measured from the trailing edge is 12.5 chords away in all directions Figure 2. Structured mesh is organized in numerical blocks in which each numerical polygon with at least 4 corners which mark as 4 block sides that are pairwise opposite to each other and a grid which is generated in ICEM-CFD with at least 430,000 nodes [8, 9]. Flow around the bi-cambered airfoil between two ridges is complex enough due to the convex and concave surface, which leads to a high-intensity pressure gradient between those two bumps. Hence, the far-field cell growth ratio is considered as 1.05. Wall $y+$ values along the airfoil surface are kept 1 to account for the low Reynolds number flow regime. The boundary layer between two ridges of the bi-camber airfoil is shown in Figure 3.

Flow domain Boundary Conditions and Fluent Solver Settings: The boundary conditions assigned to the flow domain around an airfoil as sidewall assigned with the no-slip condition while the inlet boundary condition is defined as velocity inlet and outlet boundary condition is defined as pressure outlet condition. For numerical solution implicit scheme has been usually used to solve steady flow problems and flow properties have been taken as second-order upwind and Mach number less than 0.1907. However, the assumption had been taken as incompressible flow with 1.81×10^{-5} kg/m-s as dynamic viscosity of air and 1.225 kg/m^3 as constant density and

temperature is 298 K. To solve residual equations a convergence criterion is given as 10^{-5} for all the residuals is satisfied.

Turbulence Modeling: Previous studies show that the SST K-omega model is proposed to give better separation prediction for external aerodynamic applications; this model gives better agreement with experiments of mild separated flow. This model also includes a viscosity limiter. SST k-omega turbulence model consists of two governing equations, which are based on the eddy viscosity model; this turbulence model is mainly used in aerodynamics applications. This turbulence model is a type of hybrid model that is formed by a combination of Wilcox K-epsilon model and K-omega model, therefore to simulate away from the wall K-epsilon model is used and to operate near the near-wall Wilcox model is being used at low Reynolds number of 2.1×10^6. The use of this effective feature using this model mainly depends on appropriate treatment. The performance of an airfoil is validated with an 18 cm chord length.

Results

Grid sensitivity test results: The grid sensitivity test is a tool to find the optimum number of nodes that don't affect the solver results even if there is any further increment in the number of nodes, thus using this test we can get

TABLE 1 Table of grid independency test

Number of Nodes	Coefficient of Drag (C_d)
58320	0.011148483
131730	0.009135839
234640	0.007189258
304840	0.003457691
348420	0.002794558
379420	0.002163941
401830	0.001342873
438740	0.001104262
443345	0.001104387
458420	0.001104432
469420	0.001104452

optimal grid conditions for fluent analysis studies [9]. Table 1 gives the result of the mesh independence test. The table represents data of the number of nodes vs drag coefficient. The table shows that at approx. 430k to 470k the coefficient of drag is constant; this implies that at 430k the mesh is suitable for the given design of airfoil.

Lift and drag coefficients:

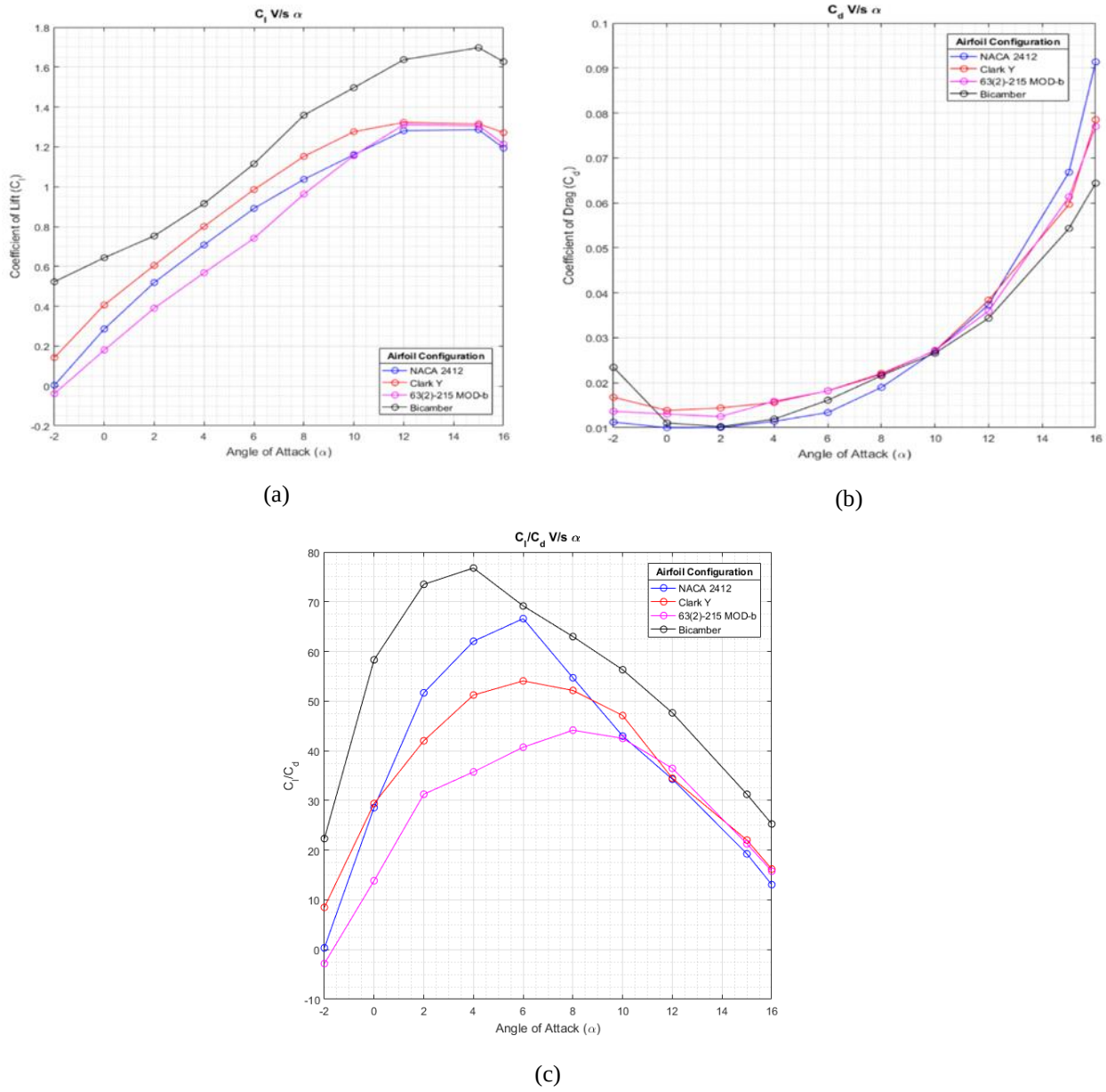

FIGURE 4 Graph between

a) Coefficient of lift (C_l) vs Angle of Attack (AOA) b) Coefficient of drag (C_d) vs Angle of Attack (AOA) (c) Cl/Cd vs Angle of Attack

Figure 4(a) represents a graph variation between drag coefficient and angle of attack of an airfoil, which represents comparative data between various airfoils that are bi-camber airfoil, NACA 2412, NACA 63(2)-215Mod-b, Clark Y. As represented in graph drag bucket value on a bi-camber airfoil is less than that of NACA 63(2)-215 MOD-b which implies drag is less on bi-camber airfoil as compared to NACA 63(2)-215 MOD-b because in bi-camber flow separates at half chord which reattaches after certain interval over the airfoil.

Figure 4(b) represents a graph variation between lift coefficient and angle of attack of an airfoil, which represents comparative data between various airfoils that are bi-camber airfoil, NACA 2412, NACA 63(2)-215Mod-b, Clark Y. As represented in graph lift coefficient value on a bi-camber airfoil is more than that of NACA 63(2)-215 MOD-b which implies lift is more on bi-camber airfoil as compared to NACA 63(2)-215 MOD-b because in bi-camber flow separates at half chord which reattaches after certain interval over the airfoil. Figure 4 (c) represents the aerodynamic efficiency of various airfoils at different angles of attack. As represented in the graph, aerodynamic

efficiency is significantly more for bi-camber airfoil at all angles of attack which shows the superiority of bi-camber airfoil design over other conventional airfoil designs.

Validation of bi-camber airfoil data by wind tunnel: The author has performed the wind tunnel model validation with the following wind tunnel specifications

- Test Section size: 600mm X 600mm X 2000mm with side windows opening on either side of test section and top opening.
- Wind tunnel Maximum Speed: 60 m/s.
- Contraction ratio: 9-10
- Honeycomb L/D: 7-9
- Wind tunnel Maximum Length: 14 meters

The wind tunnel test has been performed on a bi-camber airfoil at a velocity of 28 m/s, Reynolds number as 2 x $10^{6,}$ and at room temperature.

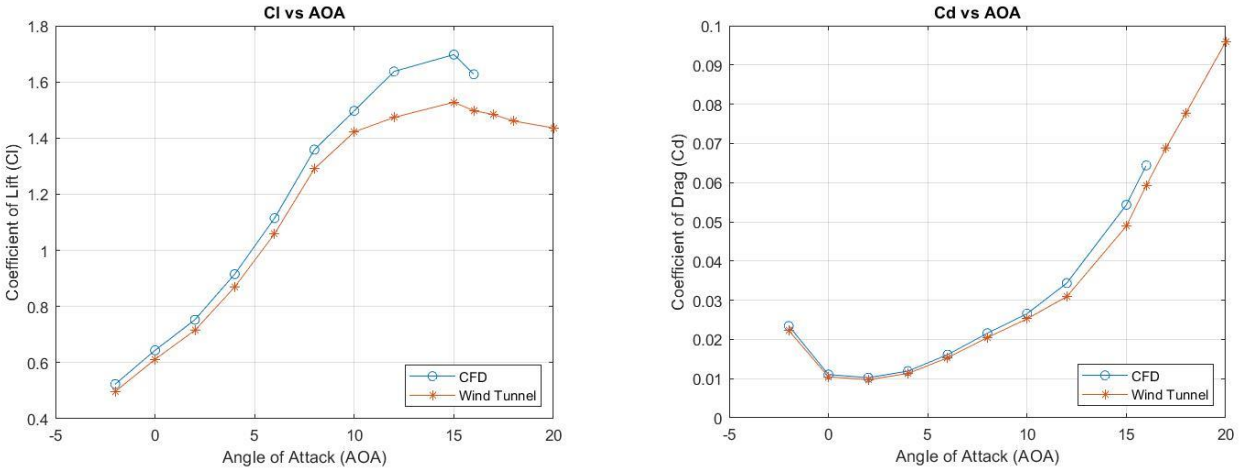

(a) (b)

FIGURE 4 Graph representation of CFD results validation from wind tunnel data

a) Coefficient of lift (C_l) vs Angle of Attack (AOA) b) Coefficient of drag (C_d) vs Angle of Attack (AOA)

Pressure Contour: Below figure 5 shows the pressure contour over a bi-camber airfoil. Blue curves over the upper surface represent the negative pressure which implies that the generate lift after the first ridge also.

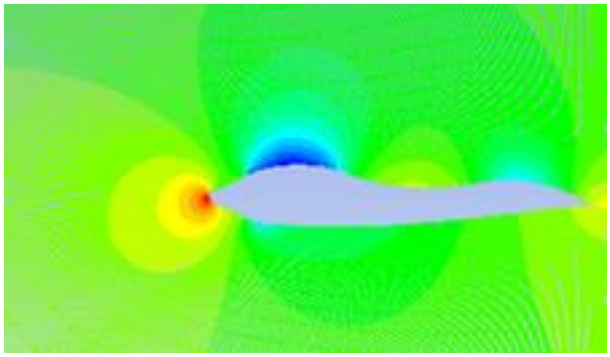

FIGURE *5* Static pressure contour over Bi-camber airfoil at 4deg AOA

Conclusion

The results obtained show, how bi-camber airfoil acts in low Reynolds number flow conditions. The flow separation occurs as the angle of attack increases on the upper surface of the airfoil but is delayed which results in a drop in lift force coefficient, and a simultaneous increment in drag force coefficient. However, in the low turbulent flow region, flow is reattached due to the second camber, which gives lift at a high angle of attack also, which is superior in aerodynamic performance over the conventional airfoil. The CFD analysis results are also validated using the wind tunnel, which reflects similar results as CFD results i.e, at a higher angle of attack lift is high.

Thus, we can conclude that bi-camber airfoil results in higher lift force and lower drag force, hence, increase the lift by drag ratio. Hence, an airfoil with a bi-camber profile is more effective than any other conventional airfoil profile.

Future Work

The currently proposed airfoil design can be altered to both the upper and lower surface of an airfoil, which could increase the efficiency for the positive and negative angle of attack. However, this research is limited to design and analysis prospects only, this research can be further carried out to get more insights.

The first and the foremost usage and development of the bi-camber can be put into the manufacturing state and can be manufactured for various commercial, military, and training aircraft. The aircraft with bi-camber airfoil will not only improve lift-drag ratio but will also work upon saving fuel and improving the speed and hence the overall efficiency of the aircraft can be improved and enhanced.

The second usage is concerned with the automotive industry where the bi-camber design can make a huge impact on the vehicles industry. All the sports and hybrid cars use the traditional single-camber streamline body design which has its disadvantages.

ACKNOWLEDGMENTS

We would also like to extend our gratitude towards the Department of Aerospace and Department of Research and Development, University of Petroleum and Energy Studies, Dehradun for their valuable support throughout the work. This paper is meant to design and analyze a software-based airfoil to spread theoretical and practical knowledge amongst the researchers. This analysis on the bi-camber airfoil profile helps students to pursue their interests and will bring ease to both the institute and students to explore different possibilities in aerodynamics.

REFERENCES

1. Yagiz, B., Kandil, O. and Pehlivanoglu, Y., 2012. Drag minimization using active and passive flow control techniques. Aerospace Science and Technology, 17(1), pp.21-31.
2. Moghaddam, T. and Neishabouri, N., 2017. On the Active and Passive Flow Separation Control Techniques over Airfoils. IOP Conference Series: Materials Science and Engineering, 248, p.012009.
3. Stanewsky, E., Delery, J., Fulker, J. and Matteis, P., 2013. Drag Reduction by Shock and Boundary Layer Control. Berlin, Heidelberg: Springer Berlin / Heidelberg.
4. Chng, T., Zhang, J. and Tsai, H., 2008. A Novel Method of Flow Injection and Suction for Lift Enhancement. 46th AIAA Aerospace Sciences Meeting and Exhibit.
5. Meunier, M., 2007. Simulation and Optimization of Flow Control Strategies for Novel High-Lift Configurations. 25th AIAA Applied Aerodynamics Conference.
6. Mahmud, Md Shamim. (2013). Analysis of the effectiveness of an airfoil with a bi-camber surface. International Journal of Engineering and Technology. 3. 569-577.
7. Frederick L. Felix, AIRFOIL WITH BICAMBERED SURFACE U.S. Patent No.5,395,071 (7 March 1995)
8. Bulat, M.P. and Bulat, P.V., 2013. Comparison of turbulence models in the calculation of supersonic separated flows. World Applied Sciences Journal, 27(10), pp.1263-1266.
9. Krishnaswamy, S., Jain, S. and Sitaram, N., 2014. Grid and turbulence model based exhaustive analysis of NACA 0012 airfoil. Journal of Advanced Research in Applied Mechanics & Computational Fluid Dynamics, 1(1), pp.13-18.